그래핀에 기초한 막의 구조와 물질 전달 성질 개관

야콥 부크하임 · 로만 비스 · 김 창 민* · 등 명 명 · 박 형 규†

취리히 연방 공과대학 기계공정공학과, *광주과학기술원 지구환경공학부
(2016년 8월 22일 접수, 2016년 8월 24일 수정, 2016년 8월 24일 채택)

Architecture and Transport Properties of Membranes out of Graphene

Jakob Buchheim, Roman M. Wyss, Chang-Min Kim*, Mengmeng Deng, and Hyung Gyu Park†

Nanoscience for Energy Technology and Sustainability, Department of Mechanical and Process Engineering,
Eidgenössische Technische Hochschule (ETH) Zürich, Zürich CH-8092, Switzerland
*School of Environmental Science and Engineering, Gwangju Institute of Science and Technology (GIST),
Gwangju 61005, Republic of Korea

(Received August 22, 2016, Revised August 24, 2016, Accepted August 24, 2016)

요 약: 최근 2차원 나노 물질을 응용하여 수처리 막의 성능을 향상시킬 수 있는가에 대한 연구가 활발하다. 그 노력의 한 가운데에 원자 두께를 가지고 있으면서 손쉽게 구할 수 있고 층으로 쌓을 수도 있는 2차원 물질인 그래핀이 자리하고 있다. 이 총설에서 우리는 그래핀으로부터 만들 수 있는 두 가지 막 구조에 관한 기초 물질 전달 현상을 최근 연구 성과를 중심으로 다룬다. 그 물질 자체로 이미 물질 전달 차단성을 갖는 그래핀에 정확히 제어된 크기의 구멍을 뚫을 수 있다면 아마도 원자 크기 수준으로 얇은 두께 때문에 그래핀 막은 같은 기공 크기의 어느 막보다도 빠른 궁극적 투과도를 나타낼 것이며, 이로부터 선택도를 담보할 수 있다면 다양한 막 분리 공정에 적용할 수 있을 것이다. 그 한 예로, 나노미터 이하의 기공을 가정한 초박막 침투성 그래핀 막에 대한 분자동력학 연구와 몇몇 초기 실험 결과들이 해수담수화 막으로서의 가능성을 보인 점은 주목할 만하다. 그래핀 물질로부터 다른 구성을 가진 막을 설계할 수 있는데, 이 막은 적당히 산화된 그래핀 마이크로 판들을 무작위로 적층함으로써 구현할 수 있다. 그래핀 판 적층 간격을 나노미터 이하로 쉽게 제어할 수 있기 때문에 이 구조 역시 수처리 및 해수담수화 막으로서의 가능성을 시사한다. 기존 막기술에 존재하지 않던 구조와 물질 전달 성질을 가짐으로써 두 종류의 그래핀 막은 앞으로 수처리 기술을 비롯한 다양한 막 기술의 응용분야에서 효과적으로 기여할 가능성이 충분하다.

Abstract: Two-dimensional materials offer unique characteristics for membrane applications to water technology. With its atomic thickness, availability and stackability, graphene in particular is attracting attention in the research and industrial communities. Here, we present a brief overview of the recent research activities in this rising topic with bringing two membrane architecture into focus. Pristine graphene in single- and polycrystallinity poses a unique diffusion barrier property for most of chemical species at broad ambient conditions. If well designed and controlled, physical and chemical perforation can turn this barrier layer to a thinnest feasible membrane that permits ultimate permeation at given pore sizes. For subcontinuum pores, both molecular dynamics simulations and experiments predict potential salt rejection to envisage a seawater desalination application. Another novel membrane architecture is a stack of individual layers of 2D materials. When graphene-based platelets are chemically modified and stacked, the interplanar spacing forms a narrow transport pathway capable of separation of solvated ions from pure water. Bearing unbeknownst permeance and selectivity, both membrane architecture - ultrathin porous graphene and stacked platelets - offer a promising prospect for new extraordinary membranes for water technology applications.

Keywords: ultrathin porous graphene, stacked graphene platelets, ultimate permeation, selectivity, water technology applications

†Corresponding author(e-mail: parkh@ethz.ch, http://orcid.org/0000-0001-8121-2344)

1. Introduction

Discovery of the atomically thin material of graphene is bringing a quantum jump to the quest of novel material and design in membrane technology. Two-dimensional (2D) nature of the graphene crystal made of hexagonally arranged, sp^2 bonded carbon atoms [1] exhibits unique material strength of unmatched stiffness and very high breaking strength[2], rendering it a widely studied material not only in solid state physics but also in fluid mechanics, mass transfer and membranology. The ultimate thinness of the material in particular implies promising applications in separation technology. Furthermore, layered architecture of graphene and graphene oxide provides a unique option for tailoring the transport selectivity.

1.1. Baffling property of graphene as a mass transfer barrier

One of the most important properties of graphene is its strong diffusion barrier characteristic. It has been found that the defect-free, single crystalline graphene lattice is impermeable to most of the gas species including H_2 and He at ambient conditions[2-4]. Furthermore, density functional theory calculations show a potential of selective atomic passage of B, N, H, O in the overall energy barrier order (~1.3 eV < 3.2 eV < 4.2 eV < 5.5 eV), with potentially predicting the boron atom passage via an intricate bond switching process such as annealing[5]. At room temperature energies, therefore, the 2D carbon crystal does not permit passage of any gas species in the lattice structure, entitling the single-atom-thick graphene an effective mass-transfer barrier[6]. For particle energies exceeding room temperature by orders of magnitude and for such miniscule particles as protons, however, molecular dynamics and experimental findings suggest that particles can indeed penetrate the graphene lattice without causing much damage to it[7,8].

These extraordinary baffling properties of graphene are currently used for corrosion inhibition coatings. Various investigations affirm unambiguous prevention of the substrate corrosion when covered with single-crystalline graphene layers[9,10]. For large-area and polycrystalline graphene coatings, however, grain boundaries and lattice defects impose a corrosion spot, for an imperfect crystal is prone to permeation of water and gases[11,12]. Localized corrosion damage at graphene grain boundaries[13] could either be patched by atomic layer deposition[10] or nullified by multiple layer graphene coating.

1.2. Transfer theory across thin membranes

For membrane technology applications, the exceptional impermeability of defect-free graphene for molecular passage implies a great opportunity to reject media by an atomically thin material. Transport of mass across graphene layers can occur primarily through pores and defects created artificially. Flow resistance of conventional manifold filters with thickness, l, is governed by viscous wall friction inside the channels and modeled by use of the classic Hagen-Poiseuille flow, a continuum mechanics solution of Navier-Stokes equations that scales the flow rate inversely proportional to l : $Q \propto l^{-1}$, where Q is the volumetric flow rate. In the absence of a channel wall and the associated friction mechanism, however, the atomically thin, porous graphene is expected to impose the least possible flow resistance to mass permeation. For mass transport of a fluid with viscosity, μ, at a differential pressure, Δp, through infinitesimally thin orifices of radius, r, only the entrance effect dominates the resistance to the flow. R. A. Sampson had found out a solution of Stokes flow through a single orifice[14] which has been extended by Tio and colleagues for a pore array of an infinitely thin disc with porosity, $\varkappa$, and coefficients $S_3 = 9.03362$, $S_5 = 5.09026$, $S_7 = 4.42312$, $S_9 = 4.19127$[15].

$$Q_{Sampson} = \frac{r^3}{3\mu}\Delta p \left(1 - \frac{2S_3}{3\pi^{5/2}}\kappa^{3/2} - \frac{6S_5}{5\pi^{7/2}}\kappa^{5/2} - \frac{18S_7}{7\pi^{9/2}}\kappa^{7/2} - \frac{56S_9}{9\pi^{11/2}}\kappa^{9/2}\dots\right)^{-1}$$

This entrance flow resistance exists at any pore entrance but neglected usually because the flow istance
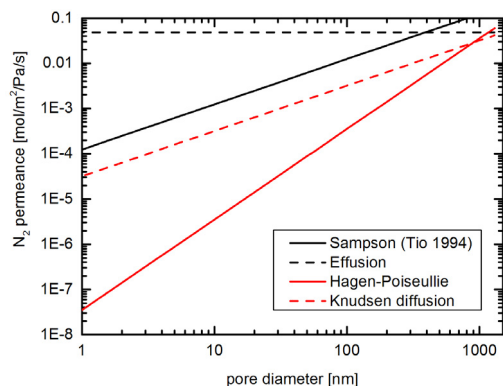
Figure 1. Comparison of different pore-flow models. Calculated flux of N2 at room temperature for various pore sizes. The membrane thickness for conventional pore-flow models (Knudsen diffusion and Hagen-Poiseuille viscous flow) is set to be 2 μm and porosity $\varkappa = 0.2$.

caused by the viscous interaction inside the channel, e.g., inner pores of a membrane, is dominant for a channel (or pore) of a finite length. In the case of an atomically thin membrane, however, it is no longer negligible.

For gases where the mean free path, l_{MFP}, of the molecules is larger than the pore diameter (Knudsen number, $Kn = l_{MFP} / 2r > 1$) the transport is governed by a free molecular flow theory. Here once again, well-known pore flow models such as Knudsen diffusion are not applicable for atomically thin porous graphene. It is not the diffusivity of the species inside the pore[16] but the odds of particles entering the pore that is responsible for the flow impedance. From the basic gas kinetic theory, the number of molecules hitting the exposed pore area depends on both the molecular number density, n, and their average thermal speed in one direction, or $\bar{u}/4$. Molecules on both sides of the orifice pore hit the pore area, and the net molecular flux across the membrane in thermal equilibrium is determined by the difference in n that can be related to a cross-membrane pressure difference, Δp. As the result, the molecular flow rate follows a formula of effusion.

$$\frac{Q_{effusion}}{V_m} = \pi r^2 \frac{\bar{u}}{4}(n_1 - n_2) = \pi r^2 \frac{\Delta p}{\sqrt{2\pi MRT}} ,$$

where V_m, M and R are the molar volume and molar mass of the transporting species and the universal gas constant, respectively.

The above equation indicates that the flow rate across an infinitely thin filter scales with $Q_{effusion} \propto r^2$ instead of $Q_{Knudsen} \propto r^3$, which means that gas flux (flow rate per unit pore area) in the free molecular flow regime will be independent of the pore size (Figure 1).

2. Mass Transport Across Porous Graphene

2.1. Pore formation

The idea of an atom-thick membrane platform that can realize non-Fickian transport across a 2D orifice has immediately engendered significant research efforts on large-scale pore formation on the otherwise impermeable graphene. Initial methods of pore formation on graphene relied on irradiation of freestanding graphene with high-energy electrons inside transmission electron microscopes (TEM). This method allows the formation of a few pores with diameters ranging from 3 Å to 20 nm[17,18]. Since the number of pores created through this method is limited, this technique was only used for solid-state pores for sequencing applications [19,20]. For membrane technology applications, however, a larger number of pores have to be achieved.

One simple way of obtaining a porous graphene membrane is to use graphene as synthesized by chemical vapor deposition (CVD). Owing to technological difficulty, CVD-grown polycrystalline graphene has defect sites along the grain boundaries of the crystal or distributed randomly on the crystalline surface. At certain CVD conditions, for example, graphene could contain nanometer-scale pinholes ranging from 1 nm to 15 nm[11] that provide the transmembrane transport pathways. These pinholes can form if catalyst substrate (e.g., Ni or Cu) has microscale roughness, scratches or surface-contamination during growth, though the detailed mechanism remains to be elucidated. Apparently, graphene is hard to nucleate or easy to bear many defects at these sites.

Artificially made defects in freestanding graphene with subnanometers in size can be realized by ultra-violet-assisted oxidative etching[21] or direct exposure to ozone[22]. Another technique to create subnanometer pores on graphene is to create sparse lattice defects by low-dose (e.g., 8 keV) Ga^+ ion irradiation followed by a weak oxidative etching, based on $KMnO_4$ and H_2SO_4, which grows subnanometer pores from the initially created defect sites[23]. A focused ion beam technology has been used to create medium-area graphene membranes with controlled pore sizes from a few nanometers to micrometers via convergent bombardment of energetic ions (Ga^+ or He^+) on a self-sustaining net of graphene[24]. A parallel process promising for large-scale pore formation is the self-assembly-driven nanolithography technique based on block-copolymer, which allows the formation of pores of a few tens of nanometers[25]. For subnanometer graphene pores the tendency of graphene healing[26] has been observed, posing a problem about long-term membrane stability. In the presence of carbon atom supply graphene tends to reform, and pores vanish. However, atomic-resolution TEM observations have shown that the presence of Si contamination which terminates graphene pore edges could greatly enhance the stability of the pores[27], an idea that might be generalized for the edge stabilization of graphene pores. Graphene regrowth is an idea worth paying attention to in combination of activation or passivation of the pore edges.

## 2.2. Transmission of liquids and ions across porous graphene

2.2.1. Theoretical studies of water transmission across porous graphene

Simulations of a liquid flow across porous graphene report remarkable permeation rates of water molecules across a graphene orifice. In a molecular dynamics (MD) simulation Suk and Aluru[28] have predicted ultrahigh permeation of water. For pore sizes around 2.7 nm, permeance of water molecules across the graphene orifice exceeds the mobility inside carbon nanotubes (CNT) or ultrathin solid-state (silicon) membranes.

Only a collective flow of water molecules in a single file inside a carbon nanotube of ~0.7 nm in diameter is faster than the transgraphene orifice transmission. The pressure drops across the graphene orifice within ~1 nm apart from the orifice surface, hinting that the primary flow impedance comes from a molecular pore-entrance event[29].

The effects of pore size and the pore edge termination have been further investigated using MD simulations[29-31]. (Note: The definition of the effective pore size may vary in the literature. Some propose to use the end of the chemical moiety, while others use the center-to-center distance of the carbon atoms as the reference points for the measurements.) For pores smaller than 4 nm the volume flow scaling per pore is roughly $Q \propto r^{3.3}$[29]. This scaling alludes to super-position of Sampson and Hagen-Poiseuille formulae may model the water permeance in this pore size and small thickness regime. All available results of MD simulations agree roughly with this scaling, $Q \propto r^x$, with x between 3 and 3.3[28-31].

The edge termination of the graphene orifice can influence the permeance for subnanometer-wide pores [30]. Cohen-Tanugi et al. have found out that hydrogenated and hydroxylated groups at the orifice mouth have strong effects. For orifices smaller than 1 nm, hydrogen-terminated pores have slightly lower per-pore permeance than hydroxyl terminated ones[30]. This effect is partially explained by the polar nature of the water molecule, which allows them to interact strongly with the hydroxyl group leading to a larger accessible area, hence a larger effective pore size (Figure 2). Another even stronger effect is that the hydrogen termination renders the orifice edge hydrophobic, which induces an artificial ordering of water molecules in the vicinity of the pore to roughen the entropic landscape and drag the traversing molecules leading to a slower flow. In contrast, the hydroxylated groups create a smoother landscape for the water molecules, as they can form hydrogen bonds themselves with the water molecules and therefore the overall water flow is increased. It appears that this argument remains to be
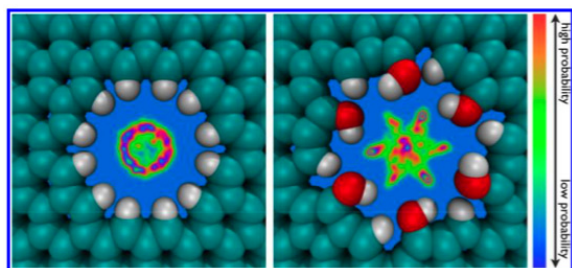
Figure 2. Oxygen density maps at inside a hydrogenated (left) and hydroxylated pore (right), with open pore areas of 23 and 28 Å^2, respectively. Light blue indicates the region in which no water oxygens are found, while red regions indicate the highest probability of finding an oxygen atom. Reprinted with permission from ref.[30]. Copyright 2012 American Chemical Society.

further scrutinized.

The pore size and pore edge termination influence the distribution of water molecules inside the pore, too. By obtaining the oxygen density maps[30,32], researchers have found out that the probability density distribution deviates from homogenous spatial distribution in bulk water depending on pore size and edge functional group (Figure 2). Similarly to water inside CNTs, water forms an ordered configuration in such confinement[30,32].

2.2.2. Water permeation experiments

Water flow across double layer graphene membranes was observed through pore sizes in the range of 50-1000 nm[24]. Celebi, Buchheim *et al*. have observed that the onset of water flow begin if both, feed and permeate, sides of the membrane are pre-wetted with liquid. If only one side is wet, capillarity prevents the onset of permeation with counterbalancing the applied transmembrane pressure difference of 2 bar or more. The measured per-pore permeance is slightly lower than the theoretical prediction of ultimate permeation but matches in scaling Sampson's model for the water flow through an orifice : $Q_{H_2O} = (r^3/3\mu_{H_2O})\Delta p$ (Figure 3). Despite membrane clogging by particulate matters, the reported flow rate for a membrane with 50-nm-wide pores is almost one-order-of-magnitude higher than conventional ultrafiltration membranes[24].
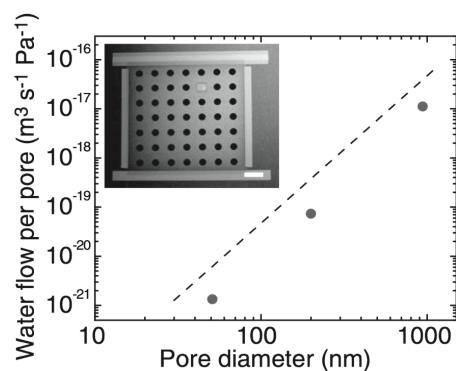
Figure 3. Water permeation data. Water flow rates per graphene pore for three graphene membranes with different pore sizes, in comparison with the modified Sampson's model prediction (dashed line). (Inset) SEM image of the Pt enclosure surrounding the entire membrane area to prevent membrane disintegration (scale bar, 10 μm). Reprinted with permission from ref.[24]. Copyright 2014 The American Association for the Advancement of Science.

The characterization of liquid flow across the graphene orifice is challenging due to clogging of the pores with sieved particles and also to the integrity of graphene with the support layer, e.g., SiN_x[24]. The latter could be improved by attaching the graphene to the support layer with directed Pt deposition to prevent the wash-off of the graphene layer (Figure 3, inset). Data from initial attempts of water flux measurement across subnanometer pores in graphene[33] bracket the expected ultrahigh flow rates predicted by the classic Sampson theory and MD simulations of Suk and Aluru[29]. By employing a twofold defect sealing method based on ALD deposition to close intrinsic graphene defects and interfacial polymerization to clog large scale tears, monolayer graphene could be transformed into a membrane allowing to measure osmotic pressure driven water flux through subnanometer pores. Subnanometer pores are made by defect creation via Ga^+ ion bombardment followed by subsequent wet chemical etching (1.875 mM $KMnO_4$ in 6.25% H_2SO_4), resulting in pores of approximate 0.48 nm in diameter. Despite the predictions that this pore size is expected to show ion rejection, NaCl (0.76 nm) passed the membrane favorably. Large-sized ions and molecules $MgSO_4$ (0.86 nm), Allura Red (~1 nm) and Dextran

(~3.7 nm) were partly rejected by this graphene membrane. However, the passage of the Dextran molecule and the pumping of NaCl indicate that defect sealing is not perfect and additional large leakage pathways through the monolayer are present, which could not be found during extensive STEM scanning[33]. These results highlight the difficulty in fabricating defect-free monolayer graphene membranes. Besides, unlike the direct physical perforation, the applicability of this method is critically limited to a monolayer of graphene.

Another method to achieve water permeable graphene monolayer was presented by Surwade and coworkers[34]. In this method monolayer single crystalline graphene, which is covering a 5-μm-wide open hole of a SiN$_x$ membrane, is treated by oxygen plasma. The exposure generates Si-terminated pores with ~1 nm in size at pore densities ranging between 10^{10} cm^{-2} and 10^{12} cm^{-2}[34]. Reported results for water permeance are, however, contradicting. Osmotic pressure driven flow through ~1 nm porous graphene yielded ~4.5 × 10^{-26} m^3/Pa/s per pore, which is very close to the Sampson's prediction of 6.4 × 10^{-26} m^3/Pa/s per pore. In a thermally driven water pervaporation measurement the observed water weight loss through the graphene membrane exceeds by orders of magnitude the predicted water permeability of porous graphene for ~20% of the devices. The mechanism for this high permeation rate remains unclear. As expected in membrane pervaporation the membrane keeps the nonvolatile ions from passage through the graphene membrane, thereby showing some potential applications for seawater desalination via membrane distillation[34].

2.2.3. Ion transport through graphene pores

MD simulations of ion transport across graphene pores show the potential of graphene as an ion selective membrane. In one simulation, hydroxyl-terminated pores with diameters of ~4 Å allowed the passage of Cl$^-$, Br$^-$ (17 : 33) but no translocation of F$^-$ or any positively charged ion species[35]. Fluor and nitrogen terminated pores, on the other hand, allowed the

passage of K$^+$, Na$^+$ and Li$^+$ at a mobility ratio of 33 : 14 : 9. Therefore, two separation mechanisms can be identified : electrostatic screening by the charge of the pore-edge functional group rejecting co-ions; and steric screening because ions with weakly bound solvation shells have higher permeation rates than strongly solvated ions[35].

Results from MD simulations of graphene pores terminated with hydroxyl groups that mimic the architecture of K$^+$ or Na$^+$ channels lends ion selective feasibility to the graphene membranes[36]. The pore mimicking the structure of a KcsA K$^+$ channel showed K$^+$ over Na$^+$ selectivity of 4. Achieving Na$^+$ selective pores, however, is more challenging. Although the graphene pore, which imitates the NavAB Na$^+$ channel preferentially bonds Na$^+$ to the dangling moiety, the transport path through the pore is too large to block other ions from translocation[36]. Further insight into ion-graphene pore interaction has been obtained by equilibrium MD simulations. The concentration, the solvation state and mobility of K$^+$ and Cl$^-$ ions inside water-filled graphene pores have been calculated[37]. The concentrations of both ion species in a carbon-terminated graphene pore are lower than the bulk counterpart, reflected by a low partition coefficient, ϕ = c_p/c_b, where c_p and c_b denote ion concentrations in the graphene pore and the bulk reservoir, respectively. For pore sizes smaller than 5 Å, c_p (thus ϕ) is practically 0. Suk and Aluru have found out that the main factor for the ion partitioning is the high free energy cost for dehydration[37] and not the dielectric exclusion as for the conventional nanofiltration membranes[38]. In addition, the diffusion constant D_p of ions under the graphene confinement is reduced compared with the bulk diffusion D_{bulk} and scaled with pore radius r : $(1/D_p\text{-}1/D_{bulk}) \propto 1/r$ leading to a remarkable drop of ϕ to ~50% inside a 5.2 Å pore[37].

Experimentally, ion diffusion measurements through graphene with subnanometer pores confirm the potential of ion selectivity and the potential of size exclusion[23]. Pores were created using ion irradiation and wet chemical etching (1.875 mM KMnO$_4$ in

6.25% H_2SO_4), which allowed for control of pore density as well as pore sizes (e.g., by duration of wet chemistry). Short etch times lead to the formation of tiny pores which show a preferential selectivity for positively charged K^+ over Cl^- presumably due to the charge at the pore edges. For slightly enlarged pores of the graphene membrane K^+ and Cl^- can pass freely, but larger dye molecules such as Allura Red with a diameter of ~1 nm cannot. Only after opening up the pores further by prolonged etching times, the dye molecules translocate the pores of the graphene[23]. The ion passage through intrinsic and artificially subnanometer defects was further investigated through ion conductance measurements[22]. Even mild ozone etching was found to create defects in the range of 3.8 Å which allow the electrokinetic passage of Na^+ and Cl^- ions. How the electromotive driving force overcome the dehydration energy penalty of the ions is elusive, partly explained if the pore size estimate was offset a little bit toward small values. This report highlights the experimental difficulty in creating nanoporous graphene, as well as the correct pore size characterization, that has the capability of ion rejection.

2.2.4. Molecular dynamics simulation of seawater desalination using porous graphene

One of the prominent applications of highly water-permeable membranes is the seawater desalination. If the relatively high water permeance can be sustained for a membrane whereas salts are rejected, such a membrane might mark an ideal platform for a future desalination process.

MD simulations of a pressurized flow of a high-salinity aqueous NaCl solution through graphene pore reveal that 100% salt rejection can be achieved for pore sizes as narrow as 5.5 Å[30]. This high rejection value for pores < 5.5 Å is observed for all pressures from 100 MPa to 225 MPa (Figure 4). For larger pores of ~9 Å in diameter the ion rejection is reduced to 80% and 40% at pressures of 100 MPa and 225 MPa, respectively (Figure 4). The latter finding is in contrast to the conventional diffusive membranes for reverse
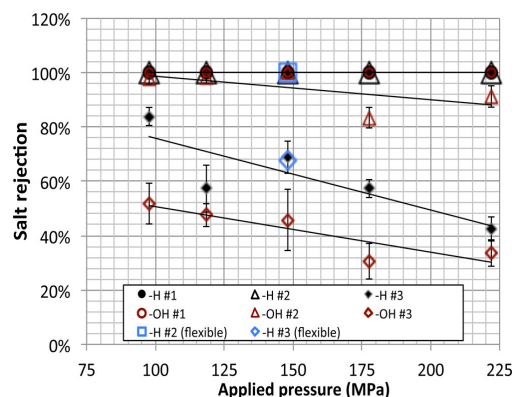

Figure 4. Average salt rejection as a function of pore type and pressure differential. The results indicate that smaller pores are capable of effectively rejecting salt but that rejection performance decreases with higher pressures. On the other hand, hydrogenated pores exhibit stronger salt rejection than hydroxylated pores. Reprinted with permission from ref.[30]. Copyright 2012 American Chemical Society.

osmosis desalination[39]. Cohen-Tanugi and Grossman argue that the large effective volume of the hydrated ion is more sensitive to pressure increase than water molecules[30]. Furthermore, a clear effect of pore edge chemistry is observed. Pores that are terminated by the polar hydroxylated group allow easy salt permeation (inferior salt rejection). The OH group on the pore edge interacts with the solvated ion similarly to the surrounding water molecules, and therefore the energy barrier for ion passage may be low[30]. In contrast, hydrogen-terminated pores show greater ion separation up to 80% for ~8 Å pores at 100 MPa.

Equilibrium MD simulations further give insights to the potential mean force (PMF) acting on the water molecules and ions at the graphene pore[40]. Na^+ ions and Cl^- have to overcome the PMF barrier of ~0.61 eV and ~0.43 eV in passing a non-functionalized graphene pore of 7.5 Å in diameter whereas water molecules face the PMF barrier of only ~0.2 eV[40]. Larger pristine graphene pores are not expected to show a significant ion rejection. In addition changes of the salinity from 0.025M to 0.25M do not change the PMF barrier significantly for non-functionalized graphene pores. In contrast, the PMF barrier of functionalized graphene pores changes with the salinity of the

electrolyte solution. The case of pore edge chemistry modification by the attachment of carboxylic groups increases the PMF for Cl^- at low ionic strength to 0.824 eV, but at high ionic strength the increased Na^+ ion concentration at the pore screens the electrostatic repulsive barrier of Cl^- yielding a relatively low PMF for the Cl^- ion passage of ~0.47 eV. The attachment of NH_3 group causes the same but reverse effect on both ion species, so that the overall passage of ions is not expected to decrease[40]. In contrast, the functionalization of the pore edge with OH groups has beneficial effects on the salt rejection performance, since it allows for high salt rejection even for as saline water as seawater[40].

One additional important factor for seawater desalination is the mechanical strength of the graphene membrane[41]. Typical reverse osmosis process pressures range from 5 MPa to 10 MPa (50-100 bar), and in order to achieve a good amount of permeate (freshwater) membranes need to sustain similar mechanical pressures. The mechanical strength of nonporous monocrystalline graphene (Young's Modulus of 1 TPa) indicates that graphene can indeed withstand high pressures if it is rendered single crystalline. Simulations have shown that porous graphene can sustain around 57 MPa if the support dimensions are carefully selected[41].

3. Mass Transport through Layered Platelets of Graphene and Graphene Oxide

3.1. Gas separation

While nanometer-scale perforation is needed to impart permeation to the otherwise impermeable 2D material, a staggered layer-by-layer stack of 2D-material platelets can create interesting architecture of molecular transport pathways. Graphene-based 2D platelets can be formed in various methods, posing highly graphitic surfaces partly mixed with a chemically derived area. A stack of pure graphene platelets forms upon van der Waals interaction (ideally ~3.4 Å in the interlayer space), thus impeding molecular passage in between

(A)

(B)
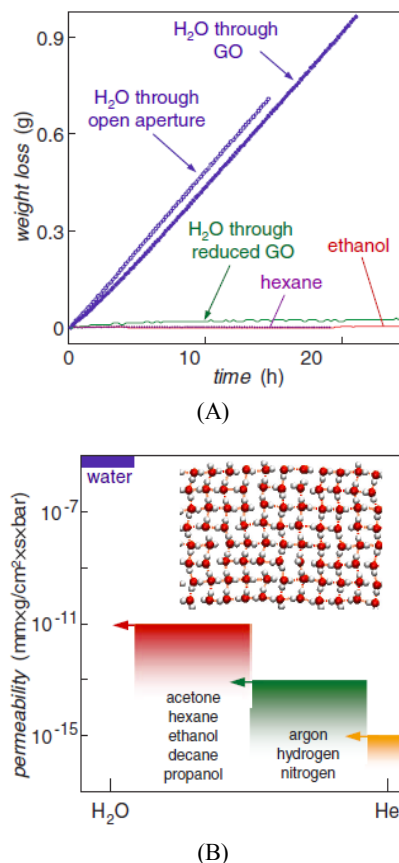
Figure 5. Permeation through GO. (A) Weight loss for a container sealed with a GO film (aperture area ≈ 1 cm^2). No loss was detected for ethanol, hexane, etc., but water evaporated from the container as freely as through an open aperture (blue curves). The measurements were carried out at room temperature in zero humidity. (B) Permeability of GO paper with respect to water and various small molecules (arrows indicate the upper limits set by experiments). (Inset) Schematic representation of the structure of monolayer water inside a graphene capillary with d = 7 Å. Adapted with permission from ref.[42]. Copyright 2012 The American Association for the Advancement of Science.

them. On the other hand, chemically derived platelets, called graphene oxide (GO), could develop molecular pillars or spacers in between the platelets during the layering process to open up space for molecular passage. Although it is challenging, the control of the GO interlayer gap will play a crucial role in various applications of chemical separation technology.

Permeation rate of water vapor through thick GO laminates (from 0.1 to 10 μm) was reported to be similar to the evaporation rate from an open-water surface

Table 1. Retention of Organic Dyes for uGNMs with Different brGO Loadings and brGO Layer Thickness. Reprinted with Permission from Ref.[45]. Copyright 2013 John Wiley and Sons

brGO loading (mg m^{-2})	Thickness (nm)	Pure water flux J_0 (L m^{-2} h^{-1} bar^{-1})	MB[a]			DR 81[a]		
			Retention (%)	J/J_0 (%)[b]	C/C_0[c]	Retention (%)	J/J_0 (%)[b]	C/C_0[c]
14.1[d]	22	21.81	99.2	90.0	1.27	99.9	89.6	1.31
17.0[e]	26	12.62	99.7	91.1	1.30	99.8	89.7	1.33
21.2[e]	33	5.00	99.7	89.4	1.32	99.9	87.2	1.33
28.3[e]	44	4.37	99.6	90.4	1.33	99.9	95.8	1.34
34.0[e]	53	3.26	99.8	95.0	1.36	99.9	95.6	1.35

[a]The concentration of feed dye solution C_0 was 0.02 mM. [b]The ratio of permeate flux of the dye solution J to the pure water flux J_0. [c]Concentration ratio of upper stream (C) when the permeation volume was 10 mL to the original feeding solution (C_0, 35 mL). [d]The applied pressure was 1 bar. [e]The applied pressure was 5 bar.
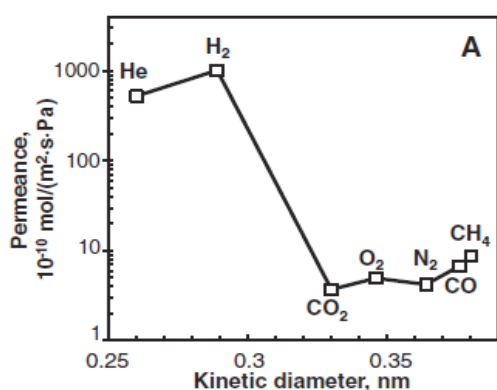
Figure 6. Single-gas permeation through GO membranes supported on porous alumina membrane at 20°C. Permeances of seven molecules through a ~18-nm-thick GO membrane. Reprinted with permission from ref.[44]. Copyright 2013 The American Association for the Advancement of Science.

under similar conditions (Figure 5A). In addition, it shows very high selectivity for water with preventing the transmission of even smaller He molecules (Figure 5B). This observation indicates that water molecules can pass through nanochannels formed between GO platelets with interacting strongly with the channel[42]. This observation triggered broad interest in research and development, along with other advantages of selectivity and ease of sample preparation. It is the stacking method or layer-interlocking strategy that has a great influence on both the gas permeability and selectivity of the GO membranes. The gas selectivity in particular can be roughly explained by a kinetic diameter argument (Figure 6), leading to a molecular sieving

mechanism. However, permeances of some gases deviate from those predictions employing the kinetic diameters, calling for further investigations[43,44].

3.2. Water permeation and separation

For the purpose of nanofiltration, base-refluxing-reduced GO (brGO) is supported by anodic aluminum oxide (AAO) substrate. The rejection for small ions, such as NaCl, Na$_2$SO$_4$, MgCl$_2$ and MgSO$_4$ is less than 60%, but for large molecules (i.e., methyl blue and direct red 81) the rejection is higher than 99% with maintaining water flux higher than commercial polymeric nanofiltration membranes (Table 1). The electrostatic interaction between graphene membrane and solutes can be explained with the Gibbs-Donnan equilibrium theory[45], and the size exclusion or the steric hindrance mechanism is under active investigation in the research community.

GO platelets and stacked membranes made out of them are prone to dispersion and disassembly in an aqueous solution, casting concerns about long-term stability as a water purification membrane material[46]. As one way to tackle this problem of membrane disintegration, polydopamine was used to bridge GO flakes and support. 1,3,5-benzenetricarbonyl trichloride was also employed to make a chemical bonding between GO flakes. The water flux was measured to be 8-27.6 L m^{-2} h^{-1} bar^{-1}. The GO membrane showed high rejection rate (> ~93% for Rodamine-WT) for large or-
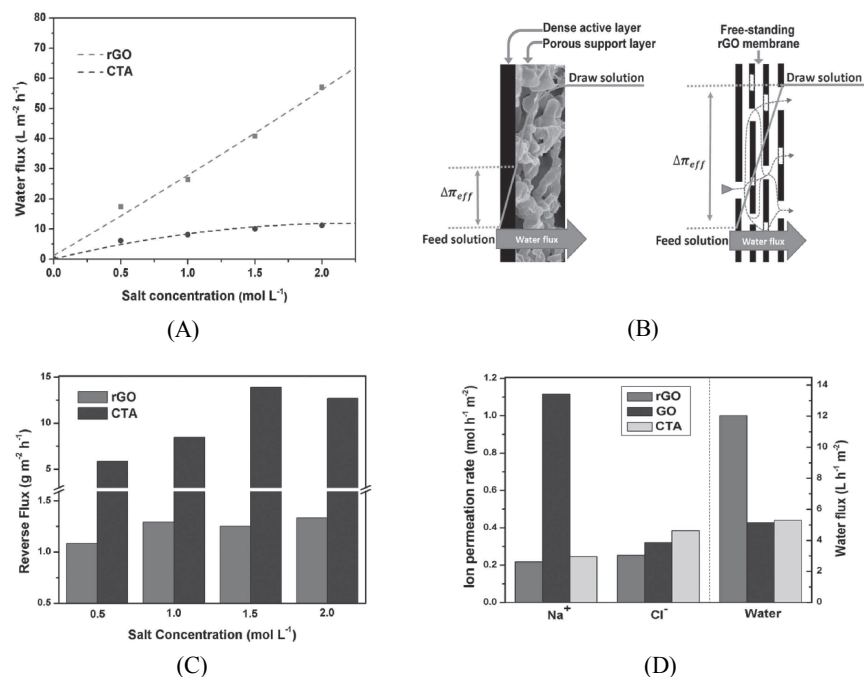
Figure 7. FO test of the freestanding rGO membrane. (A) Variations of water fluxes of the freestanding rGO (100 nm thick) and commercial HTI CTA membranes as a function of salt (draw solution) concentrations. (B) Comparison of the osmotic pressure profiles for the conventional supported membrane (left) and freestanding rGO (right) membrane in FO process. For rGO membranes, the intrinsic defects (i.e., holes and wrinkles) act as the channels for mass transport. (C) Variations of reverse salt fluxes of the freestanding rGO (100 nm thick) and commercial HTI CTA membranes as a function of salt (draw solution) concentrations. (D) Permeation rates of Na^+ and Cl^- and water fluxes through rGO, GO, and CTA membranes using NaCl as feed solution and ammonia as draw solution, respectively. Reprinted with permission from ref.[49]. Copyright 2014 John Wiley and Sons.

ganic molecules whereas the rejection for small ions was poor (6-19% for NaCl) when the system was pressurized. Interestingly, both water flux and salt rejection are not a strong function of the number of GO layers. This finding implies that even a very thin GO membrane could in principle separate ions and organic matters in water. In addition, the degree of ion rejection diminishes with the ion concentration, attributed to the change of Debye length and supportive of a charge exclusion mechanism[47].

In contrast to previous reports, if GO is placed on alumina filters during the preparation method of vacuum filtration, membranes maintained great stability in water without any interlayer bonding agent. The micrometers-thick GO membranes prepared in this way have shown selective transport towards water only, a similar result to water vapor transport across GO membranes

of similar thicknesses. Ions with large hydrated radii can be separated via size exclusion. Charge of ions or molecules, however, did not play a decisive role in the separation, which is supported by an observation that permeation rate of AsO_4^{3-} was almost identical to that of Na^+ or Cl^-[48]. This observation hints that electrostatic interaction may get much weakened in so-called a charge-neutralized environment caused by insertion of aluminum cations in the interspace of GO platelets.

Forward osmosis (FO) is another water technology application of the stacked 2D membranes. For an FO process a freestanding reduced GO (rGO) membrane has shown a promising result. Freestanding rGO membranes show high permeance (57.0 L m^{-2} h^{-1} when DI water and NaCl (2.0 M) were used as feed and draw solutions, respectively) than a commercial FO membrane (CTA membrane, ~10 L m^{-2} h^{-1} at the same con-

ditions) (Figure 7A). This finding is particularly important because freestanding rGO membranes could eliminate the most problematic issue of an internal concentration polarization of the FO process, leading to an increase in the effective chemical potential difference (Figure 7B). Importantly, the reverse salt flux (from draw to feed) in g m^{-2} h^{-1} is lower for this membrane, and so the salt rejection capability of rGO membranes is greater than that of CTA (Figure 7C, D)[49].

3.3. Theoretical investigation

Theoretical modeling could explain the origin of the superior performance of the stacked graphene architecture and predict new processes and applications. Based on the first-principle simulation, the ultrafast permeation of water through the graphene stack has been attributed to the unique hydrogen bonding (HB) configuration under the tight nanoscale 2D confinement. Even though the interlayer spacing is as narrow as 10 Å, the average HB number per water molecule is comparable to that of bulk water. However, the effect of perturbation appears to be localized only at the graphene-water interface, thereby weakening the molecular dipole moment and the hydrogen bonding of water at the interface with also changing the tilting angle of the molecule. As the result, the water mobility can be enhanced in this nanometer-confined environment[50].

On the other hand, phase inversion of water molecules from liquid to solid (ice) in the nanoconfined 2D channel was suspected as a major reason for anomalous transport of water through the stacked-graphene channels. Unlike other molecules such as He, Ar, N$_2$, and H$_2$, only water molecules can change the phase in the highly confined graphitic channel because of the unique HB constellation of water. The long range order of the ice network is energetically much more favored than liquid water inside the 2D confinement. Thus, the formation of ice will promote a collective motion of water molecules in between graphene layers with less friction, rendering easy passage of water through the graphene interlayer channels. According to the simulation results, the formation of an ice bilayer is favored is the interlayer distance becomes a bit wider (7 to 10 Å), explained by lower energy barriers of the ice bilayer[51].

A possibility of a molecular slip flow within the interlayer graphene channel has been predicted theoretically. Because of the intrinsic smoothness and crystallinity of graphene, molecules could slide over graphene sheets easily. Comparison of the slip lengths of other liquid species (i.e., Ar and CH$_4$) with that of water reveals that water has much longer slip length regardless of the flow regime. The slip lengths for liquid Ar, CH$_4$ and water have been reported to be 11 ± 1 nm, 5.9 ± 0.6 nm and 60 ± 6 nm, respectively[52].

The ultrafast and highly selective transport properties that the stacked-graphene architecture pose are an outcome of nanometer-sized tight confinement, innate properties of graphene, and the unique fluid properties under the confinement. Particularly, water in the confined channels, whether it is driven from liquid or gas phases, has manifested a unique transport behavior disparate from the other species. Hence, the stacked-graphene-platelet architecture has great potential for fundamental investigations and applications in various areas which demand high performance standards in selectivity and permeation.

4. Conclusions

High permeance and great selectivity are the primary properties generally desired for membrane materials for separation technology, although they counteract each other to form a tradeoff line in the selectivity-permeance diagram. Porous graphene, a perforated membrane out of mono- or few-layer graphene, can be mechanically robust and offer ultimate permeation to a transmitting species. It poses potential for use in water purification and seawater desalination if perforation is made with subnanometer precision and at maximal areal porosity. The edge chemistry of the orifices (or pores) has a significant primary effect on pronounced selectivity of the membrane, yet it also influences the

permeance of water through the membrane. Another filtration-membrane architecture of a stack of graphene or graphene-oxide platelets can also be realized and rendered stable in an aqueous environment by various self-adhering ways, to offer great selectivity towards water and weakly charged small ions. The selectivity of the stacked-GO-platelet membrane can be controllable by tailoring the interlayer distance with chemical reduction and oxidation and is governed largely by coulombic exclusion, size exclusion and steric hindrance.

Porous 2D layer and stacked platelets are two design architectures bearing the potential for embodying ultra-permeable and highly-selective membranes, respectively. If combined in a rational design, a synergistic membrane architecture for an extremely efficient water treatment could be obtained. To this end, a great deal of experimental and theoretical investigations need be carried out to deepen our understandings of the nano-material properties and the mechanisms of transport and selection. At the same time, manufacturing options need be searched and established for cost-effective large-scale production of these membranes.

Reference

1. K. S. Novoselov, A. K. Geim, S. V. Morozov, D. Jiang, Y. Zhang, S. V. Dubonos, I. V. Grigorieva, and A. A. Firsov, "Electric field effect in atomically thin carbon films", *Science*, **306**, 666 (2004).

2. O. Leenaerts, B. Partoens, and F. M. Peeters, "Graphene: A perfect nanoballoon", *Appl. Phys. Lett.*, **93**, 193107 (2008).

3. J. S. Bunch, S. S. Verbridge, J. S. Alden, A. M. Van Der Zande, J. M. Parpia, H. G. Craighead, and P. L. McEuen, "Impermeable atomic membranes from graphene sheets", *Nano Letters*, **8**, 2458 (2008).

4. T. Georgiou, L. Britnell, P. Blake, R. V. Gorbachev, A. Gholinia, A. K. Geim, C. Casiraghi, and K. S. Novoselov, "Graphene bubbles with controllable curvature", *Appl. Phys. Lett.*, **99**, 093103 (2011).

5. L. Tsetseris and S. T. Pantelides, "Graphene: An impermeable or selectively permeable membrane for atomic species?", *Carbon*, **67**, 58 (2014).

6. V. Berry, "Impermeability of graphene and its applications", *Carbon*, **62**, 1 (2013).

7. O. Lehtinen, J. Kotakoski, A. V. Krasheninnikov, A. Tolvanen, K. Nordlund, and J. Keinonen, "Effects of ion bombardment on a two-dimensional target: Atomistic simulations of graphene irradiation", *Phys. Rev. B - Cond. Mat. Mater. Phys.*, **81**, 153401 (2010).

8. S. Hu, M. Lozada-Hidalgo, F. C. Wang, A. Mishchenko, F. Schedin, R. R. Nair, E. W. Hill, D. W. Boukhvalov, M. I. Katsnelson, R. A. Dryfe, I. V. Grigorieva, H. A. Wu, and A. K. Geim, "Proton transport through one-atom-thick crystals", *Nature*, **516**, 227 (2014).

9. S. Chen, L. Brown, M. Levendorf, W. Cai, S.-Y. Ju, J. Edgeworth, X. Li, C. W. Magnuson, A. Velamakanni, R. D. Piner, J. Kang, J. Park, and R. S. Ruoff, "Oxidation resistance of graphene-coated Cu and Cu/Ni alloy", *ACS Nano*, **5**, 1321 (2011).

10. Y.-P. Hsieh, M. Hofmann, K.-W. Chang, J. G. Jhu, Y.-Y. Li, K. Y. Chen, C. C. Yang, W.-S. Chang, and L.-C. Chen, "Complete corrosion inhibition through graphene defect passivation", *ACS Nano*, **8**, 443 (2014).

11. S. C. O'Hern, C. A. Stewart, M. S. H. Boutilier, J.-C. Idrobo, S. Bhaviripudi, S. K. Das, J. Kong, T. Laoui, M. Atieh, and R. Karnik, "Selective molecular transport through intrinsic defects in a single layer of CVD graphene", *ACS Nano*, **6**, 10130 (2012).

12. T. Yoon, J. H. Mun, B. J. Cho, and T. S. Kim, "Penetration and lateral diffusion characteristics of polycrystalline graphene barriers", *Nanoscale*, **6**, 151 (2014).

13. M. Schriver, W. Regan, W. J. Gannett, A. M. Zaniewski, M. F. Crommie, and A. Zettl, "Graphene as a long-term metal oxidation barrier: worse than nothing", *ACS Nano*, **7**, 5763 (2013).

14. R. A. Sampson, "On Stokes´s current function",

Proc. Natl. Acad. Sci. U.S.A., **182**, 449 (1891).

15. K.-K. Tio and S. S. Sadhal, "Boundary conditions for stokes flows near a porous membrane", *Appl. Sci. Re*s., **52**, 1 (1994).

16. M. Knudsen, "Die Molekularströmung der Gase durch Offnungen und die Effusion", *Ann. Phys.*, **333**, 999 (1909).

17. M. D. Fischbein and M. Drndić, "Electron beam nanosculpting of suspended graphene sheets", *Appl. Phys. Lett.*, **93**, 113107 (2008).

18. C. J. Russo and J. A. Golovchenko, "Atom-by-atom nucleation and growth of graphene nanopores", *Proc. Natl. Acad. Sci. U.S.A.*, **109**, 5953 (2012).

19. C. A. Merchant, K. Healy, M. Wanunu, V. Ray, N. Peterman, J. Bartel, M. D. Fischbein, K. Venta, Z. Luo, A. T. C. Johnson, and M. Drndic, "DNA translocation through graphene nanopores", *Nano. Lett.*, **10**, 2915 (2010).

20. G. F. Schneider, S. W. Kowalczyk, V. E. Calado, G. Pandraud, H. W. Zandbergen, L. M. K. Vandersypen, and C. Dekker, "DNA translocation through graphene nanopores", *Nano. Lett.*, **10**, 3163 (2010).

21. S. P. Koenig, L. Wang, J. Pellegrino, and J. S. Bunch, "Selective molecular sieving through porous graphene", *Nat. Nanotechnol.*, **7**, 728 (2012).

22. M. I. Walker, R. S. Weatherup, N. A. W. Bell, S. Hofmann, and U. F. Keyser, "Free-standing graphene membranes on glass nanopores for ionic current measurements", *Appl. Phys. Lett.*, **106**, 023119 (2015).

23. S. C. O'Hern, M. S. Boutilier, J. C. Idrobo, Y. Song, J. Kong, T. Laoui, M. Atieh, and R. Karnik, "Selective ionic transport through tunable sub-nanometer pores in single-layer graphene membranes", *Nano Lett.*, **14**, 1234 (2014).

24. K. Celebi, J. Buchheim, R. M. Wyss, A. Droudian, P. Gasser, I. Shorubalko, J. I. Kye, C. Lee, and H. G. Park, "Ultimate permeation across atomically thin porous graphene", *Science*, **344**, 289 (2014).

25. J. Bai, X. Zhong, S. Jiang, Y. Huang, and X. Duan, "Graphene nanomesh", *Nat. Nanotechnol.*, **5**, 190 (2010).

26. R. Zan, Q. M. Ramasse, U. Bangert, and K. S. Novoselov, "Graphene reknits its holes", *Nano Lett.*, **12**, 3936 (2012).

27. J. Lee, Z. Yang, W. Zhou, S. J. Pennycook, S. T. Pantelides, and M. F. Chisholm, "Stabilization of graphene nanopore", *Proc. Natl. Acad. Sci. U.S.A.*, **111**, 7522 (2014).

28. M. E. Suk and N. R. Aluru, "Water transport through ultrathin graphene", *J. Phys. Chem. Lett.*, **1**, 1590 (2010).

29. M. E. Suk and N. R. Aluru, "Molecular and continuum hydrodynamics in graphene nanopores", *RSC Adv.*, **3**, 9365 (2013).

30. D. Cohen-Tanugi and J. C. Grossman, "Water desalination across nanoporous graphene", *Nano Lett.*, **12**, 3602 (2012).

31. D. Zhou, Y. Cui, P. W. Xiao, M. Y. Jiang, and B. H. Han, "A general and scalable synthesis approach to porous graphene", *Nat. Commun.*, **5**, 4716 (2014).

32. C. Zhu, H. Li, and S. Meng, "Transport behavior of water molecules through two-dimensional nanopores", *J. Chem. Phys.*, **141**, 18 (2014).

33. S. C. O'Hern, D. Jang, S. Bose, J. C. Idrobo, Y. Song, T. Laoui, J. Kong, and R. Karnik, "Nanofiltration across defect-sealed nanoporous monolayer graphene", *Nano Lett.*, **15**, 3254 (2015).

34. S. P. Surwade, S. N. Smirnov, I. V. Vlassiouk, R. R. Unocic, G. M. Veith, S. Dai, and S. M. Mahurin, "Water desalination using nanoporous single-layer graphene", *Nat. Nanotechnol.*, **10**, 459 (2015).

35. K. Sint, B. Wang, and P. Král, "Selective ion passage through functionalized graphene nanopores", *J. Am. Chem. Soc.*, **130**, 16448 (2008).

36. Z. He, J. Zhou, X. Lu, and B. Corry, "Bioinspired graphene nanopores with voltage-tunable ion selectivity for Na+ and K+", *ACS Nano*, **7**, 10148 (2013).

37. M. E. Suk and N. R. Aluru, "Ion transport in sub-5-nm graphene nanopores", *J. Phys. Chem.*,

140, 084707 (2014).

38. A. E. Yaroshchuk, "Dielectric exclusion of ions from membranes", *Adv. Colloid Interfac*, **85**, 193 (2000).

39. M. E. Williams, "A review of reverse osmosis theory", http://www.eetcorp.com/heepm/RO_TheoryE, (2003).

40. D. Konatham, J. Yu, T. A. Ho, and A. Striolo, "Simulation insights for graphene-based water desalination membranes", *Langmuir*, **29**, 11884 (2013).

41. D. Cohen-Tanugi and J. C. Grossman, "Mechanical strength of nanoporous graphene as a desalination membrane", *Nano Lett.*, **14**, 6171 (2014).

42. R. R. Nair, H. A. Wu, P. N. Jayaram, I. V. Grigorieva, and A. K. Geim, "Unimpeded permeation of water through helium-leak-tight graphene-based membranes", *Science*, **335**, 442 (2012).

43. H. W. Kim, H. W. Yoon, S. M. Yoon, B. M. Yoo, B. K. Ahn, Y. H. Cho, H. J. Shin, H. Yang, U. Paik, S. Kwon, J. Y. Choi, and H. B. Park, "Selective gas transport through few-layered graphene and graphene oxide membranes", *Science*, **342**, 91 (2013).

44. H. Li, Z. Song, X. Zhang, Y. Huang, S. Li, Y. Mao, H. J. Ploehn, Y. Bao, and M. Yu, "Ultrathin, molecular-sieving graphene oxide membranes for selective hydrogen separation", *Science*, **342**, 95 (2013).

45. Y. Han, Z. Xu, and C. Gao, "Ultrathin graphene nanofiltration membrane for water purification", *Adv. Funct. Mater.*, **23**, 3693 (2013).

46. C. N. Yeh, K. Raidongia, J. J. Shao, Q. H. Yang, and J. X. Huang, "On the origin of the stability of graphene oxide membranes in water", *Nat. Chem.*, **7**, 166 (2015).

47. M. Hu and B. Mi, "Enabling graphene oxide nanosheets as water separation membranes", *Environ. Sci. Technol.*, **47**, 3715 (2013).

48. R. K. Joshi, P. Carbone, F. C. Wang, V. G. Kravets, Y. Su, I. V. Grigorieva, H. A. Wu, A. K. Geim, and R. R. Nair, "Precise and ultrafast molecular sieving through graphene oxide membranes", *Science*, **343**, 752 (2014).

49. H. Liu, H. Wang, and X. Zhang, "Facile fabrication of freestanding ultrathin reduced graphene oxide membranes for water purification", *Adv. Mater.*, **27**, 249 (2015).

50. G. Cicero, J. C. Grossman, E. Schwegler, F. Gygi, and G. Galli, "Water confined in nanotubes and between graphene sheets: a first principle study", *J. Am. Chem. Soc.*, **130**, 1871 (2008).

51. D. W. Boukhvalov, M. I. Katsnelson, and Y. W. Son, "Origin of anomalous water permeation through graphene oxide membrane", *Nano Lett.*, **13**, 3930 (2013).

52. S. K. Kannam, B. D. Todd, J. S. Hansen, and P. J. Daivis, "Slip flow in graphene nanochannels", J. *Chem. Phys.*, **135**, 144701 (2011).